Particle size distribution for additive manufacturing powder using stereological corrections

C. Gallagher[*], E. Kerr, S. McFadden

Faculty of Computing, Engineering and the Built Environment, Ulster University, Derry/Londonderry BT48 7JL, UK.

HIGHLIGHTS

- Feedstock particle size distributions are key for metal additive manufacturing.
- Standard mounting methods introduce significant errors in particle size estimation.
- Stereological corrections are identified that improve size distribution estimates.
- 2,280 particle cross-sections are analysed in the size range of 9–76 μm.
- Stereologically corrected distributions are comparative to laser diffraction data.

GRAPHICAL ABSTRACT
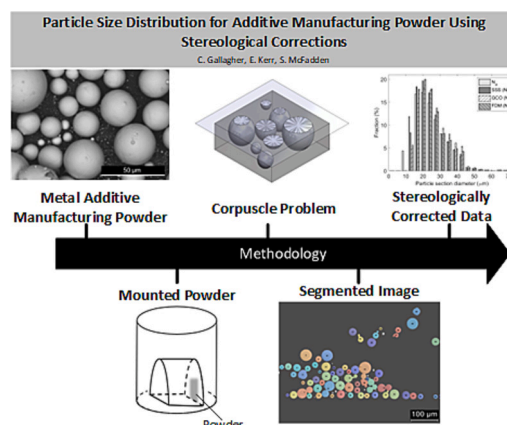
ARTICLE INFO

ABSTRACT

Additive manufacturing powders require well-defined Particle Size Distributions (PSDs) and spherical morphology for good powder flowability. To simplify characterisation processes, powders can be prepared using standard metallurgical preparation techniques, followed by optical imaging to determine the PSD of cross-sectioned particles. However, this measured PSD typically provides underestimates of the true diameters; hence, stereological corrections must be applied. Three stereological correction methods: the Scheil-Schwartz-Saltykov (SSS) method; the Goldsmith and Cruz-Orive (GCO) method and a Finite Difference Method (FDM) are assessed. Laser Size Diffraction (LSD) analysis provided the ground truth data. Particle cross-sections of 2,280 powder particles (Ti-6Al-4V) were analysed in the size range of 9–76 μm. The mean absolute errors were found to be 2.3% for the SSS method, 2.4% for the GCO method, and 1.6% for the FDM method. Hence, whilst all three methods provided an improved estimate of the PSD, FDM was determined the most effective method in this case.

* Corresponding author.
   E-mail address: Gallagher-c64@ulster.ac.uk (C. Gallagher).

1. Introduction

For good manufacturability, additive manufacturing powders must adhere to many stringent technical requirements. These requirements include the need for the powder to have the correct composition, low porosity, a well-graded particle size distribution, and spherical morphology, to name a few. The latter two of these requirements are desired to ensure good flowability of the powder [1,2]. Good powder flowability allows for a thin layer of powder (typically 25 to 60 μm) to be uniformly spread across the powder bed during the recoating stage of the Powder Bed Fusion (PBF) process [3]. To reduce costs, powder in the PBF process is typically reused after blending with fresh powder in order to maintain the technical requirements of the process [4]. The powder needs to be monitored and checked at regular stages in the reuse cycle. In the laser-based powder-blown Directed Energy Deposition (DED) additive manufacturing process, higher percentages of larger particles in the size distribution have been found to increase flow resistance [5]; hence, monitoring and controlling the particle size distribution is important.

Various particle size analysis methods exist, such as laser diffraction, photon-correlation spectroscopy, sedimentation, and sieving techniques, of which laser diffraction is widely accepted as an industry standard approach [6]. Most of these techniques use an effect of particle size, such as light scattering, rather than direct measurement of the particles themselves. Scanning Electron Microscopy (SEM), with its large depth of focus, can be used to take images of loose powder to analyse morphology and size distribution but powder containment within the vacuum chamber of the SEM becomes an issue, therefore, conductive tape is regularly used to adhere the powder to the sample stage. In a similar way to SEM, advanced optical microscopes (3D digital microscopes) with autofocus zoom and *Z*-stacking capability can capture images of tape-mounted powders, but issues arise with the lighting methods and glare from the bright metal particles [7].

Particle sizes for powders used in the Laser-Based Powder Bed Fusion (L-PBF) process are typically in the range of 10–60 μm, whereas the particle size range for Electron Beam Powder Bed Fusion (EB-PBF) processes is typically 60–105 μm [8]. Harkin et al. [4] performed laser diffraction analysis on powder samples used in the L-PBF process and found the particle size distribution range was 14.5–76 μm. Shanbhag and Vlasea [9] used Dynamic Image Analysis to determine the size distribution of powder used in the EB-PBF process, which was found to be in the range of 45–105 μm.

Many users of powder-based additive manufacturing processes are small and medium-sized enterprises (SMEs) and, hence, typically do not have direct access to standard particle size analysis methods. To ensure that powders remain within specification between part builds, the need to outsource analysis of powders arises. Outsourcing, however, typically results in increased costs and lead times. It would therefore be beneficial to these SMEs if a lower-cost method was developed for determining the size distribution of the powder particles using in-house equipment that may already be available for metallurgical preparation purposes.

In metallography using optical (light-based) methods, there is a requirement to secure the sample so that it can be ground and polished with a flat surface. This allows for improved focussing on the observation plane. As the magnification increases, the depth of focus decreases, and the requirement for flatness becomes more important. Samples are routinely mounted in a polymer matrix to secure the sample. Grinding and polishing of the sample is performed to obtain a flat observation plane within the specimen. This method of mounting, grinding, and polishing is used for qualitative analyses of metal powder particles and is useful for confirming the particle morphology in a powder reuse regime to determine the presence of spatter particles from the process [10]. An issue arises with any attempt to make a quantitative analysis of the powder particle size distribution on a single dissecting plane. Any measurement of size distribution of the measured cross sections will likely be an underestimate of the true particle size. This is known as the corpuscle problem and it arises due to the fact that the observation plane is unlikely to dissect the diametral plane of the particle to reveal its true size. The cross section of a sphere through any plane other than the diametral plane will give a circle of smaller diameter than the diameter of the sphere itself. If the 3D particle size distribution is to be estimated from the measured cross sections, a stereological unfolding procedure must be applied to the 2D distribution.

Stereology involves the use of statistical methods, integral geometry and probability, for relating measured 2D dimensions to parameters defining a 3D structure [11,12]. The theoretical derivation of many stereological methods is based on the probability that sections of a given size are produced when a particle is intercepted by a plane. This probability may be calculated as follows:

$$p(r_1 < r < r_2) = \frac{1}{R}\left(\sqrt{R^2 - r_1^2} - \sqrt{R^2 - r_2^2}\right) \tag{1}$$

Where R is the actual radius of the sphere, r_1 and r_2 are the lower and upper limits, respectively, of the defined interval of apparent section sizes, and p is the probability of cutting sections within this defined interval.

Assuming a large number of spherical particles are distributed uniformly in space, two main biases are produced in any stereological method [13,14]. The first is related to the fact that a section will only have a diameter equal to the true particle diameter if the sectioning plane happens to pass through the diametral plane of the particles measured. Rather, the centres of the particles will lie distant from the sectioning plane and thus produce sections with a diameter smaller than that of the true particle diameter. This bias is referred to as the Sectioning Bias [15]. The second stereological bias is concerned with the probability of a sectioning plane intersecting a particle. This probability is proportional to the particle diameter; therefore, larger particles have a greater probability of being sectioned by the plane than smaller particles and thus, being represented by particle sections on the sectioning plane. The 2D size distribution therefore shifts towards larger diameters. This bias is known as the Emerging Bias [15].

There are two main approaches to determining the true size distribution from an apparent size distribution. One approach involves fitting a continuous parametric Probability Density Function (PDF) to the data [16], while the second approach involves the use of finite histograms with a bin size of Δ [17]. However, differences arise in published literature where some authors place R in Eq. (1), with some placing R at the upper limit of each class (bin) interval [11,17], whilst others place R at the central (median) value of each bin interval [12,18]. The focus of this manuscript is on the finite histogram methods, presenting the frequency tables in histograms using bins of adequate size.

The aim of this work is to establish appropriate stereological correction methods for determining the particle size distribution of additive manufacturing powders from images of cross-sectioned particles. Several stereological techniques are investigated, namely, the Scheil-Schwartz-Saltykov technique [19] (commonly referred to as the Saltykov method); the Goldsmith [14] and Cruz-Orive [20,21] method; and the Finite Difference Method (FDM) developed by Harayama [22] as applied by Basak and Sengupta [23]. The current work is based on application to virgin powder particles (that is, unprocessed feedstock powder) with the assumption that all particles are spherical and hence produce no shape related ambiguities. To determine the accuracy of the method, the output from each stereological correction is compared to Laser Size Diffraction (LSD) benchmark data of the powder, which is considered an industry standard method of determining particle size distribution.

2. Materials and methods

The powder used in this study was plasma atomised Grade 23 Ti-6Al-4V titanium alloy. This alloy with 6 wt% aluminium and 4 wt%

vanadium is widely used as an additive manufacturing powder. Grade 23 is a composition defined as an Extra Low Interstitial grade due to tighter restrictions being placed on elements O, N and H, that, when present in small quantities, go into interstitial solid solution in the titanium alloy matrix. Grade 23 titanium alloy is used widely in the biomedical sector. It should be stated that the composition of the powder is not a consideration in this analysis. The proposed analysis is applicable to any grade of material with spherical morphology.

2.1. Sample preparation

A sample of powder was spread on the sample stage of a hot-mounting press before backfilling with Bakelite mounting powder. A standard cylindrical sample, of 40 mm diameter, was produced upon completion of the hot-mounting cycle in which the initial powder sample was infiltrated into the Bakelite to a depth of approximately 100 μm, on the bottom, flat face of the cylinder. The mounted sample was then cut along its axial direction, and one of the resulting halves of the cylinder repositioned on the sample stage of the hot-mounting press at 90^0 orientation to that of the original mounting cycle. This repositioned sample was again backfilled with Bakelite powder and the hot-mounting cycle was repeated to remount the sample so that the initial Ti-6Al-4V powder layer was aligned along the axial direction of the new cylindrical sample. A schematic diagram depicting the remounting procedure is provided in Fig. 1.

The purpose of rotating and remounting the sample was to reduce the chance of grinding through the original layer of powder infiltrated on the bottom face of the original mounted sample. Furthermore, this remounting procedure minimizes the effects of small-scale information loss which may arise due to the grinding out of smaller particles that may have settled on the sample stage of the hot-mounting press when in the original orientation (leading to a bias similar to that of the emerging bias).

Grinding, using P2500 SiC paper, and polishing stages were performed using a semi-automatic grinding and polishing machine with complementary rotation. Fine polishing was performed using water-based 1-μm diamond suspension.

2.2. Digital imaging and image analysis

A compound microscope with fixed lens was used to perform digital imaging under brightfield illumination. Images were captured at 200× magnification, resulting in a scale of one pixel equating to approximately 0.3 μm. An example of a captured image is shown in Fig. 2(a). Analysis of captured images was conducted using MATLAB.

Watershed segmentation is an image segmentation algorithm used in image processing and computer vision to separate objects or regions of interest in an image by treating it as a topographic map, where the image intensity is considered as the elevation [24]. Otsu thresholding is an automated method used in image processing to determine an optimal threshold value for image segmentation without prior knowledge of the image. The Otsu algorithm calculates the threshold that minimizes the intra-class variance of pixel intensities, effectively separating the foreground and background of an image [25]. An image analysis algorithm based on the Watershed Segmentation method [24] and Otsu thresholding [25] was used to segment images to obtain individual particles as objects. Particles intersecting image boundaries were removed and manual post-processing of the images was conducted to remove any erroneously identified particles from the dataset. See Fig. 2(b) for an example of the output of the segmentation algorithm. A total of 2,280 particle cross-sections were analysed. Individual particle cross-sections were not measured multiple times.

2.3. Determination of the particle size distribution

LSD of a sample of the powder was conducted to give a ground truth for comparison purposes. The apparent particle size distribution was generated from the images of the cross-sectioned particles via automated image analysis. The cross-sectional area of each particle was converted into an apparent diameter by means of the equivalent circular diameter. This is a common procedure having the advantage that it is orientation independent, unlike direct measurement of the feret diameter which can produce variance depending on the angle of the diameter being measured [26,27].

The area of interest (AOI) was considered a unit area; hence, the apparent particle size distribution data was normalised with respect to the AOI. The apparent particle size distribution data was then presented in histogram format using arithmetic binning with groups of equal class widths, and the stereological correction methods applied based on the following assumptions:

(i) All particles are spherical in shape.
(ii) Particles are homogenously distributed in space.
(iii) The maximum apparent diameter on the cross-sectional plane is equal to the diameter of the largest particle.

3. Stereological corrections

Wicksell [13] first considered the Corpuscle Problem, adopting a mathematician's viewpoint based on differential calculus. Wicksell considered the probability of finding the apparent diameter, d_i, centred within a bin to derive a transformation matrix for 15 bins. The bins were defined by Wicksell as follows: $1/4^{th}$ bin (range: $0 - 0.5\Delta$); 1st bin (range: $0.5\Delta - 1.5\Delta$); i^{th} bin (range: $(i - 0.5)\Delta - (i + 0.5)\Delta$)); and 15th bin (range: $14.5\Delta - 15.5\Delta$); with the size distribution expressed via the median value in each bin, i.e. $0.25\Delta, \Delta, …, i\Delta, …, 15\Delta$. Several others have since attempted to apply and improve Wicksell's results. Saltykov [28] proposed a method of successive subtraction through further development of Schwartz's [29] modification of Scheil's [30] method, based on an experimentalist's viewpoint. Saltykov used different bin ranges compared to Wicksell of: 1st bin (range: $0 - \Delta$); i^{th} bin (range: $(i - 1)\Delta - i\Delta$)); and 15th bin (range: $14\Delta - 15\Delta$); and instead expressed the size distribution of particles in terms of the upper bin limit value for each respective bin, i.e. $\Delta, …, i\Delta, …, 15\Delta$. The Saltykov method has become one of the most commonly used methods of unfolding a 2D size distribution to determine the true 3D size distribution. However, both Goldsmith [14] and Cruz-Orive [20,21] independently improved these methods by presenting a method which combines the experimentalists' and mathematicians' viewpoints, using the same bin ranges as Saltykov, but expressing the size distribution in terms of the median value of each bin (like Wicksell's original method). It is the coefficients calculated using the method proposed independently by Goldsmith and Cruz-Orive that are recommended for practical use [31]. Ueda [15] attempted to improve the method by Goldsmith and Cruz-Orive for distributions possessing a wide range of particle sizes, typically expressed in a log-
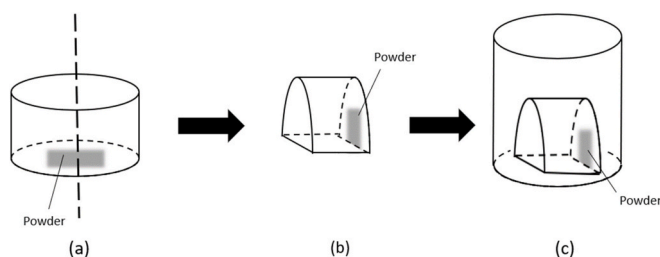

Fig. 1. Schematic diagram depicting the remounting process stages (a) the original cylinder of Bakelite with the powder layer infiltrated on the bottom face, (b) after cutting the original cylinder along the axial direction and rotating one half of the cut sample and (c) remounting within a new Bakelite cylinder so that the powder layer is aligned along the axial direction.

(a)

(b)
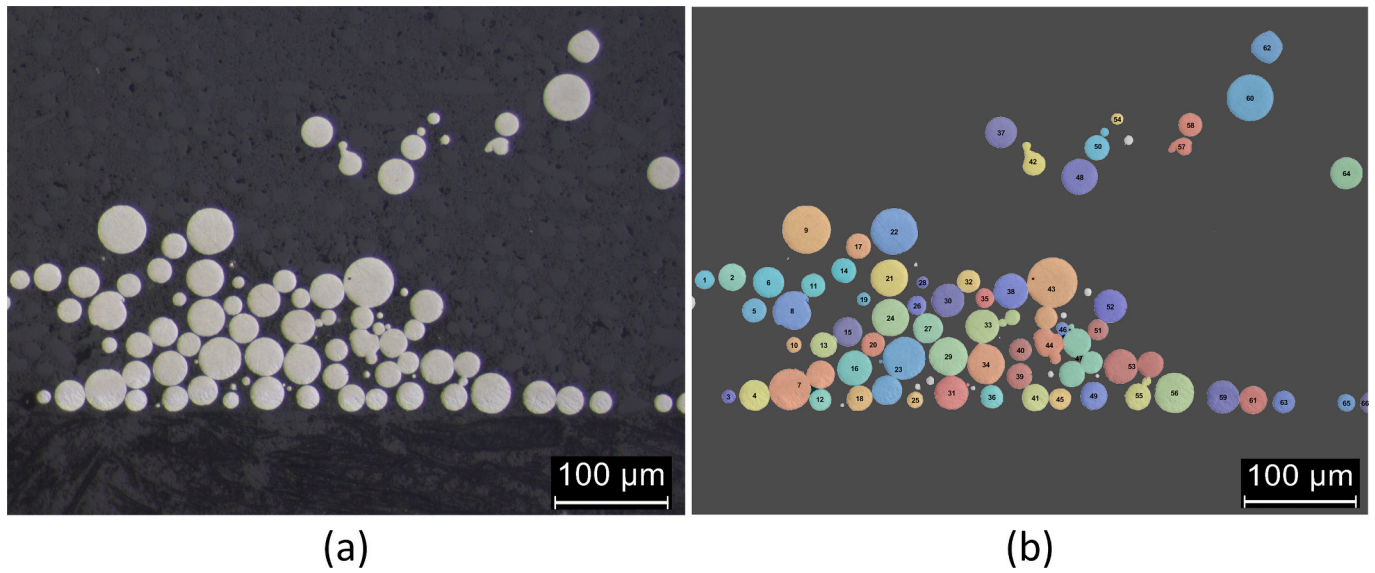
Fig. 2. Digital images of the cross-sectioned Ti-6Al-4V particles (a) after fine polishing performed using water-based 1-μm diamond suspension and (b) after application of the image segmentation algorithm.

normal graph using arbitrarily configurable size classes. Other methods involve an analytical solution of an integral equation such as in the method proposed by Harayama [22] using the Finite Difference Method (FDM).

In this study, three different variations of stereological correction were applied to the data. These methods were the commonly used Scheil-Schwartz-Saltykov method (SSS) [19]; the Goldsmith [14] and Cruz-Orive [21] method (GCO); and a finite difference method (FDM) developed by Harayama [22] as applied by Basak and Sengupta [23].

3.1. The Sheil-Schwartz-Saltykov method (SSS)

The Scheil-Schwartz-Saltykov method is commonly referred to as the Saltykov method and is based on Eq. (2).

$$N_a(i) = \Delta \sum_{j=1}^{k} N_v(j) \left(\sqrt{j^2 - (i-1)^2} - \sqrt{j^2 - i^2} \right) \tag{2}$$

Where $N_a(i)$ is the number of particle sections in class i per unit area of the intersection plane, $N_v(j)$ is the number of particles in class j per unit volume of the sample, Δ is the class (bin) width and k is the number of size classes (number of bins), for which $k\Delta = d_{max}$, where d_{max} is the maximum diameter of the measured sections. This method uses the probability of obtaining a section with apparent diameter between the bin boundaries of $d_{i-1} = (i-1)\Delta$ and $d_i = i\Delta$ from a sphere possessing a true diameter $D_j = j\Delta$. The general formula of the Saltykov method uses a successive subtraction process, given by the following:

$$N_v(j) = \frac{1}{\Delta} (\alpha(j,j)N_a(j) - \alpha(j+1,j)N_a(j+1) - \ldots - \alpha(k,j)N_a(k)) \tag{3}$$

Which can be written in summation form as follows:

$$N_v(j) = \frac{1}{\Delta} \sum_{i=j}^{k} \alpha(i,j)N_a(i) \tag{4}$$

Takahashi and Suito [32] have generalised the $\alpha(j,i)$ values by following the procedure proposed by Saltykov as:

$$\alpha(j,i) = \begin{cases} T(i,i) & \forall(i=j) \\ -\sum_{m=i}^{j-1} \alpha(m,i)T(m,j) & \forall(i<j) \end{cases} \tag{5}$$

Where $T(i,j)$ is the translation coefficient and is defined as follows:

$$T\left(i,j\right) = \begin{cases} \dfrac{1}{A_{SSS}(j,j)} & \forall(i=j) \\ \dfrac{A_{SSS}(i,j)}{A_{SSS}(j,j)} & \forall(i<j) \end{cases} \tag{6}$$

$A_{SSS}(i,j)$ are known as the shape factor and they are determined by the successive substitution of integer values of i and j into:

$$A_{SSS}(i,j) = \sqrt{j^2 - (i-1)^2} - \sqrt{j^2 - i^2} \ \forall(i \leq j) \tag{7}$$

3.2. Goldsmith and Cruz-Orive method (GCO)

Goldsmith [14] and Cruz-Orive [20,21] each independently improved previous methods through using the same bin ranges as Saltykov [17] but describing the distribution using the centre values of each bin, that is $D_j = (j - 1/2)\Delta$. Hence, the size distribution of the particles can be determined from the size distribution of the apparent diameters using:

$$N_v(j) = \frac{1}{\Delta} \sum_{i=1}^{N} P^{ji} N_a(i) \tag{8}$$

Where P^{ji} is the inverse of P_{ij} described as follows:

$$P_{ij} = \begin{cases} \sqrt{(j-1/2)^2 - (i-1)^2} - \sqrt{(j-1/2)^2 - i^2} & \forall j = 1, \ldots, i-1 \\ \sqrt{i - 3/4} & \forall j = i \end{cases} \tag{9}$$

3.3. Finite difference method (FDM)

Using the finite difference method, based on a probabilistic approach, Harayama [22] proposed a method of determining the true 3D particle size distribution from the 2D sectional size distribution by analytical solution of the integral equation:

$$N_a(x) = \int_{x}^{\infty} p(x) \bullet N_v(z)dz \tag{10}$$

Where $p(x)$ is the probability a particle of diameter z will produce a circle with diameter between x and $x + dx$ on a sectioning plane within a cube of unit length and is given by:

$$p(x) = \frac{x}{\sqrt{z^2 - x^2}} \quad \forall x \leq z \tag{11}$$

As $N_v(z)$ is the unknown quantity in Eq. (10) and $N_a(x)$ is the known quantity, Eq. (10) may be considered as a Volterra equation of the second kind. For an arbitrary diameter u, solution of this equation is found by:

$$N_v(u) = -\frac{2}{\pi} \bullet \frac{d}{du} \int_u^\infty \frac{N_a(x)}{\sqrt{x^2 - z^2}} dx \tag{12}$$

Assuming the groups are arranged in arithmetic progression, and letting Δ be the class width, applying FDM on Eq. (12), and subsequently integrating, gives for the jth group:

$$N_v(j)\Delta = A_{FDM}(j,j)N_a(j) + \sum_{i=j+1}^{k} A_{FDM}(i,j)N_a(i) \tag{13}$$

Where,

$$A_{FDM}(j,j) = \begin{cases} 1 & \forall (j = 1) \\ \frac{2}{\pi} ln\left(\frac{j + \sqrt{j^2 - (j-1)^2}}{j - 1}\right) & \forall (j > 1) \end{cases} \tag{14a}$$

$$A_{FDM}\left(i,j\right) = \frac{2}{\pi} ln\left(\frac{i + \sqrt{i^2 - (j-1)^2}}{i + \sqrt{i^2 - j^2}} \times \frac{i - 1 + \sqrt{(i-1)^2 - j^2}}{i - 1 + \sqrt{(i-1)^2 - (j-1)^2}}\right) \forall (i > j) \tag{14b}$$

Each method was coded in MATLAB and the relevant histograms and cumulative frequency graphs output to enable comparison between each method and with LSD analysis.

3.4. Comparison of stereological corrections

As LSD analysis is one of the industry standard methods of determining the true particle size distribution of a powder, the results from LSD analysis were used as the benchmark data to determine which method of stereological correction best approximates the true particle size distribution. To assess this, the Mean Absolute Error (MAE) between the LSD data and each stereological correction output was calculated. This calculation involved finding the sum of the absolute differences between the LSD cumulative size distribution and the cumulative size distributions from the stereological corrections for each D_j value (from each bin) and dividing by the number of bins, as follows:

$$MAE = \frac{1}{k} \sum_{i=1}^{k} |N_E - N_{GT}| \tag{15}$$

Where k is the number of bins, N_{GT} represents the assumed ground truth taken as the cumulative fraction values, N_v, from the LSD size distribution, and N_E represents the relevant cumulative fraction values of the estimates that are being compared to the ground truth. The N_E value can be taken as the cumulative N_a fraction values for the apparent cumulative size distribution or the respective cumulative N_v fraction values from the distributions obtained from each stereological correction method. As the LSD analysis data used different bins than those used for the apparent particle size distribution and for each stereological correction, the LSD data was interpolated using linear interpolation to determine the ground truth for error estimation at the upper and central bin values, as appropriate.

The mean, standard deviation, skewness and kurtosis values were also calculated for each size distribution. The purpose of calculating the skewness and kurtosis values is to show comparison across higher order statistical measures to enable more in depth comparisons. As these measures have a tendency to be more sensitive to change, they provide a more granular indication of similarity than standard deviation.

4. Results

As shown in Fig. 3, the apparent particle size distribution (N_a) has greater fractions of smaller particles than that of the LSD size distribution. Hence, the apparent size distribution of the particle sections is an underestimate of the true particle size distribution, obtained from LSD, thereby highlighting the need for stereological corrections to be applied to the apparent particle size distribution data. Fig. 3(a) shows the data in histogram format whilst Fig. 3(b) shows the cumulative size distributions.

The resulting size distributions obtained after applying the stereological corrections to the apparent size distribution (N_a) are shown in Fig. 4, in histogram format, using 20 bins. It can be seen that the size distributions for each stereological correction (SSS, GCO, and FDM) have shifted to the right compared to the 2D sectional size distribution (N_a), producing greater fractions of particles of larger diameter, as expected. This is further evidenced in Fig. 5, which shows the cumulative line graphs for the 2D apparent diameters size distribution (N_a), and for LSD analysis, as in Fig. 3(b), with the addition of the cumulative size distributions after application of each stereological correction method (SSS, GCO, and FDM).

Measures of central tendency and dispersion of the data for each size distribution were then calculated and the results are displayed in Table 1. The values D_{10}, D_{50} and D_{90} represent the diameters at which the cumulative values are 0.1, 0.5 and 0.9, respectively. The calculated error values are also provided in Table 1.

5. Discussion

The use of discrete binning of particle size has the advantages that data can be easily collected from direct measurement of sizes of sections; the number of particles of a specific size are obtained quantitatively; and the method is distribution free, meaning the user does not need to make a priori assumptions about the type of distribution. However, a trade-off exists in that smaller class sizes provide a better approximation of the true size distribution, but larger class sizes provide greater numerical stability. As yet, no method for determining the optimal class size exists. In this study, 20 bins were used, resulting in a class size of 3.7 μm.

The method of further improving the GCO method by Ueda [15] was not investigated in this study as Ueda states their method is not recommended where the uniformity coefficient, U_C, of the 2D distribution is <3.5. The formula for the uniformity coefficient is $U_c = d_{60}/d_{10}$, where d_{60} and d_{10} are the diameters with a 0.6 and a 0.1 cumulative rate, respectively. In this study, it was found that $U_c = 1.9$.

The particle size range was found to be between 9 μm and 76 μm. Given that this size range aligns with the size distributions found using LSD by Harkin et al. [4] for powders used in L-PBF (14.5–76 μm), and by Shanbhag and Vlasea [9] for EB-PBF powders using digital image analysis (45–105 μm), the efficacy of the proposed method in determining the size distribution of powders used in additive manufacturing processes has been demonstrated. The mean particle size calculated from the apparent particle size distribution was 23.7 μm. The size distribution obtained from LSD analysis was used as the ground truth data for the true particle size distribution, for which the mean particle size was found to be 27.9 μm. In comparison, the mean particle size obtained after both the SSS method and the GCO method of stereological correction was 26.5 μm, whereas the FDM method resulted in a mean particle size of 27.0 μm. Therefore, the errors in the mean particle sizes from each distribution, compared to the LSD benchmark data, were found to be 15.0% for the apparent size distribution (difference of 4.2 μm), 5.0% for both the SSS and GCO methods of stereological correction (difference of 1.4 μm), and 3.2% for the FDM method (difference of 0.9
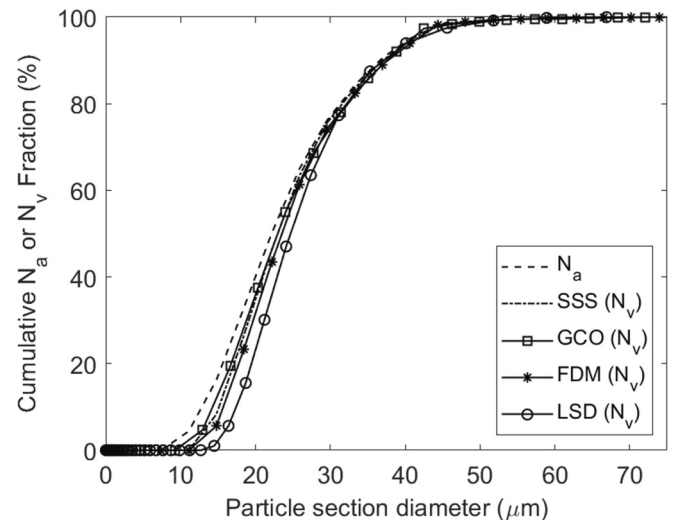
(a)

(b)
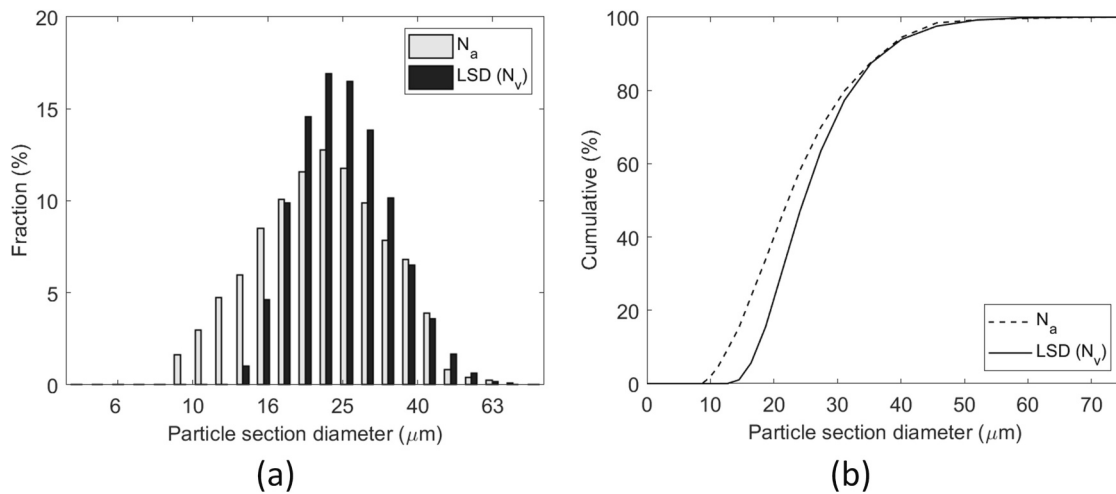
Fig. 3. (a) Histogram depicting the binned fractions of apparent particle diameters and the true particle diameters as determined via laser size diffraction (LSD) analysis, (b) the corresponding cumulative size distributions, highlighting how the size of apparent diameters are typically smaller than the true particle diameter and hence the need for stereological corrections.
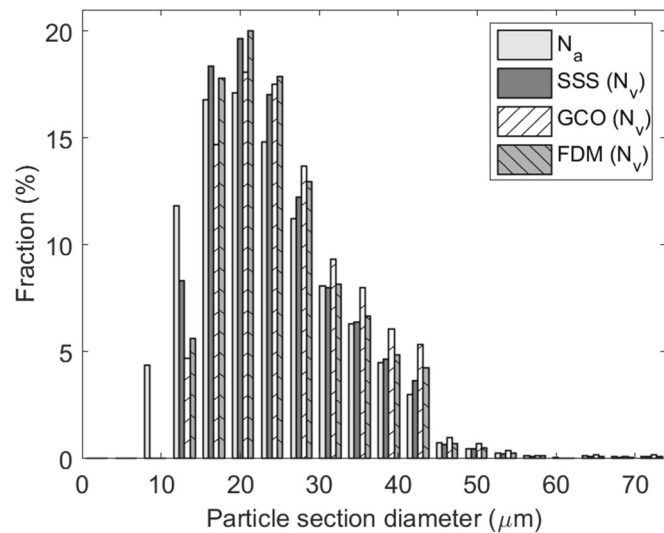
Fig. 4. Comparison of apparent 2D section size distribution to 3D particle size distribution after stereological correction using the Scheil-Schwartz-Saltykov (SSS) method, the Goldsmith and Cruz-Orive (GCO) method and the finite difference method (FDM).

Fig. 5. Cumulative line graphs comparing the particle size distribution obtained from the 2D apparent section sizes to the benchmark laser size diffraction (LSD) particle size distribution and the 3D particle size distributions obtained via stereological corrections using the Scheil-Schwartz-Saltykov (SSS) method, the Goldsmith and Cruz-Orive (GCO) method and the finite difference method (FDM).

μm). Hence, on preliminary analysis of the mean particle sizes alone, an improvement is seen in the estimation of the true particle size upon application of stereological corrections to the apparent particle size distribution.

However, Mean Absolute Error (MAE) provides a more comprehensive view of the errors across the entire distribution as it involves calculating the errors for each bin and then calculating the mean value of these errors, therefore providing a better measure of fit. MAE was used in this study as it is a widely used metric for evaluating the performance of predictive models, providing a simple, intuitive, robust measure of assessing prediction accuracy. MAE is also less sensitive to outliers compared to other errors such as the mean squared error (MSE). The MAE values were found to be 3.6% for the apparent particle size distribution (N_a), 2.3% for the SSS method of stereological correction, 2.4% for the GCO method of stereological correction, and 1.6% for the FDM method of stereological correction. Therefore, although both the SSS and GCO methods resulted in a mean particle size of 26.5 μm, comparing the MAE of each (2.3% for SSS and 2.4% for GCO) shows that

Table 1
Table containing statistical measures of central tendency and dispersion for each particle size distribution.

	N_a	SSS (N_v)	GCO (N_v)	FDM (N_v)	LSD (N_v)
Mean (μm)	23.7	26.5	26.5	27.0	27.9
Standard Deviation (μm)	9.3	8.6	9.0	8.6	8.0
Skewness (−)	0.9	1.0	1.0	1.0	1.1
Kurtosis (−)	4.3	4.5	4.5	4.6	4.6
D_{10} (μm)	12.8	15.1	14.3	15.7	17.4
D_{50} (μm)	22.1	23.0	23.0	23.5	24.7
D_{90} (μm)	36.6	37.0	37.6	37.7	37.2
Mean Absolute Error (MAE) (%)	3.6	2.3	2.4	1.6	–

the SSS method provides a slightly better overall fit across the distribution to that of the LSD distribution than the GCO method in this study.

Furthermore, it is encouraging to observe that the higher-order statistical measures (skewness and kurtosis) are similar for all three methods and that they tend towards the values measured for the LSD method. Given that higher order statistics are more sensitive to change, the agreement of this data demonstrates the efficacy of the stereology corrections.

As the FDM method resulted in the smallest MAE value of the three stereological methods assessed, it appears to be the method which best approximates the true particle size distribution in this study.

6. Conclusion

Three different stereological correction methods were assessed to determine the accuracy with which each method describes the true particle size distribution by unfolding the size distribution of a sample of cross-sectioned particles. Laser size diffraction (LSD) analysis of a sample of the powder was used as the ground truth for benchmarking the results from the application of the stereological methods analysed. The stereological corrections assessed in this study were the Scheil-Schwartz-Saltykov (SSS) method (commonly referred to as the Saltykov method), the Goldsmith and Cruz-Orive (GCO) method, and a Finite Difference Method (FDM). As expected, all three methods produce a size distribution with larger particle sizes than that of the apparent diameters of cross-sectioned particles. However, they still appear to produce an underestimate of the true particle size distribution, as defined by the LSD analysis performed on the powder.

The proposition of a method of cross-sectioning particles and applying stereological corrections to the measured size distribution of apparent diameters may be used as an effective method for estimating the 3D particle size distribution. The significance of this study is that the method of powder mounting, grinding, polishing, and imaging is extended beyond a qualitative particle morphology analysis. The method of stereological correction on data from 2D sections (which could be argued as semi-quantitative) provides a route towards a fully quantitative method for characterising 3D particle size distributions in powders. It is envisaged that the methodology proposed here will assist those small to medium sized enterprises who have metallurgical preparation and basic optical microscopy (a compound microscope) to extend their powder analysis capability at a reduced cost base and with minimal capital investment. SEM technology is orders of magnitude more expensive than optical microscopy to install and maintain. Advanced 3D digital microscopy is currently more expensive than standard-issue compound microscopy. The application of the methodology outlined here will assist those enterprises in integrating particle sizing into their quality assurance workflows and processes. The approach should also reduce (not replace) the frequency with which powder characterisation needs to be outsourced to laboratories with specialist equipment such as LSD. All stereological methods cited here are recommended but overall, in this study, the FDM method provided the optimum estimation of the true particle size distribution when compared to LSD data.

Future work would involve the application of these stereological correction methods to determine the efficacy of the approach for powders produced from alternative manufacturing processes (gas atomisation, plasma-rotating electrode processing, ultrasonic processing, etc.,) and for powders that have been reused in previous builds within the L-PBF process that contain irregular particles from the spatter of the melt pool [10].

CRediT authorship contribution statement

C. Gallagher: Conceptualization, Methodology, Software, Validation, Formal analysis, Investigation, Data curation, Writing – original draft, Writing – review & editing, Visualization. **E. Kerr:** Conceptualization, Writing – review & editing, Supervision. **S. McFadden:** Conceptualization, Resources, Writing – review & editing, Supervision, Project administration.

Declaration of Competing Interest

The authors declare that they have no known competing financial interests or personal relationships that could have appeared to influence the work reported in this paper.

Data availability

Data will be made available on request.

References

[1] A.G. Stavrou, C. Hare, A. Hassanpour, C. Wu, Investigation of powder flowability at low stresses: influence of particle size and size distribution, Powder Technol. 364 (2020) 98–114.

[2] Y. Zhao, Y. Cui, Y. Hasebe, H. Bian, K. Yamanaka, K. Aoyagi, T. Hagisawa, A. Chiba, Controlling factors determining flowability of powders for additive manufacturing: a combined experimental and simulation study, Powder Technol. 393 (2021) 482–493.

[3] S.E. Brika, M. Letenneur, C.A. Dion, V. Brailovski, Influence of particle morphology and size distribution on the powder flowability and laser powder bed fusion manufacturability of Ti-6Al-4V alloy, Addit. Manufact. 31 (2020) 100929.

[4] R. Harkin, H. Wu, S. Nikam, J. Quinn, S. McFadden, Reuse of grade 23 Ti6Al4V powder during the laser-based powder bed fusion process, Metals. 10 (2020) 1700.

[5] A.D. Iams, M.Z. Gao, A. Shetty, T.A. Palmer, Influence of particle size on powder rheology and effects on mass flow during directed energy deposition additive manufacturing, Powder Technol. 396 (2022) 316–326.

[6] D. Susan, Stereological analysis of spherical particles: experimental assessment and comparison to laser diffraction, metallurgical and materials transactions, Phys. Metall. Mater. Sci. 36 (2005) 2481–2492.

[7] C. Gallagher, R. Harkin, E. Kerr, S. McFadden, Examining the quality of new and reused powder in the powder bed fusion process via optical microscopy, in: Proceedings of the 38th International Manufacturing Conference (IMC38), 2022, pp. 89–96.

[8] T. DebRoy, H.L. Wei, J.S. Zuback, T. Mukherjee, J.W. Elmer, J.O. Milewski, A. M. Beese, A. Wilson-Heid, A. De, W. Zhang, Additive manufacturing of metallic components – process, structure and properties, Prog. Mater. Sci. 92 (2018) 112–224.

[9] G. Shanbhag, M. Vlasea, Powder reuse cycles in electron beam powder bed fusion—variation of powder characteristics, Materials 14 (2021) 4602.

[10] R. Harkin, H. Wu, S. Nikam, J. Quinn, S. McFadden, Analysis of spatter removal by sieving during a powder-bed fusion manufacturing campaign in grade 23 titanium alloy, Metals. 11 (2021) 399.

[11] D.L. Sahagian, A.A. Proussevitch, 3D particle size distributions from 2D observations: stereology for natural applications, J. Volcanol. Geotherm. Res. 84 (1998) 173–196.

[12] M.A. Lopez-Sanchez, S. Llana-Fúnez, An extension of the Saltykov method to quantify 3D grain size distributions in mylonites, J. Struct. Geol. 93 (2016) 149–161.

[13] S.D. Wicksell, The corpuscle problem: a mathematical study of a biometric problem, Biometrika 17 (1925) 84.

[14] P.L. Goldsmith, The calculation of true particle size distributions from the sizes observed in a thin slice, Br. J. Appl. Phys. 18 (1967) 813–830.

[15] T. Ueda, An improved Goldsmith-Cruz-Orive method for estimation of spherical size distribution from sectional size distribution, suitable for arbitrary size classes, Powder Technol. 388 (2021) 412–417.

[16] D. Depriester, R. Kubler, Resolution of the Wicksell's equation by minimum distance estimation, Image Anal. Stereol. 38 (2019) 213–226.

[17] S.A. Saltikov, The Determination of the Size Distribution of Particles in an Opaque Material from a Measurement of the Size Distribution of their Sections, Stereology, Springer Berlin Heidelberg, Berlin, Heidelberg, 1967, pp. 163–173.

[18] M.D. Higgins, Measurement of crystal size distributions, Am. Mineral. 85 (2000) 1105–1116.

[19] S.A. Saltykov, Sterometric Metallurgy, Part 2, 1961.

[20] L.M. Cruz-Orive, Particle size-shape distributions: the general spheroid problem. I. Mathematical model, J. Microsc. (Oxford) 107 (1976) 235–253.

[21] L. Cruz-Orive, Particle size-shape distributions: the general spheroid problem: II. Stochastic model and practical guide, J. Microsc. (Oxford) 112 (1978) 153–167.

[22] Y. Harayama, Determining the size distribution of spherical particles dispersed in a material from the measured diameter distribution of sections on a sample plane, Res. Mech. 16 (1985) 263–277.

[23] C.B. Basak, A.K. Sengupta, Development of a FDM based code to determine the 3-D size distribution of homogeneously dispersed spherical second phase from microstructure: a case study on nodular cast iron, Scr. Mater. 51 (2004) 255–260.

[24] T. Breckon, C. Solomon, Fundamentals of Digital Image Processing: A Practical Approach Using Matlab, Wiley-Blackwell, 2011.

[25] N. Otsu, A threshold selection method from gray-level histograms, IEEE Trans. Syst. Man Cybernet. 9 (1979) 62–66.

[26] R. Heilbronner, D. Bruhn, The influence of three-dimensional grain size distributions on the rheology of polyphase rocks, J. Struct. Geol. 20 (1998) 695–705.

[27] A. Berger, M. Herwegh, J. Schwarz, B. Putlitz, Quantitative analysis of crystal/grain sizes and their distributions in 2D and 3D, J. Struct. Geol. 33 (2011) 1751–1763.

[28] S.A. Saltykov, Calculation of the Distribution Curve for the Size of Dispersed Grains 15, Plant Laboratory, 1949, pp. 1317–1319.

[29] H.A. Schwartz, The metallographic determination of the size distribution of temper carbon nodules, Metals Alloys 5 (1934) 139–141.

[30] E. Scheil, Die Berechnung der Anzahl und Größenverteilung kugelförmiger Kristalle in undurchsichtigen Körpern mit Hilfe der durch einen ebenen Schnitt erhaltenen Schnittkreise, Zeitschrift für anorganische Chemie (Leipzig, Germany: 1892) vol. 201, 1931, pp. 259–264.

[31] J.C. Russ, Practical Stereology, Plenum Press, New York, 1986.

[32] J. Takahashi, H. Suito, Evaluation of the accuracy of the three-dimensional size distribution estimated from the Schwartz-Saltykov method, metallurgical and materials transactions, Phys. Metall. Mater. Sci. 34 (2003) 171–181.